Role of fastenings in modifying the hysteretic response of panel-to-panel joints for CLT structures

Role of fastenings in modifying the hysteretic response of panel-to-panel joints for CLT structures

Luca Marchi [(1)], Francesca Ferretti [(2)], Luca Pozza [(2*)], Roberto Scotta [(1)]

[(1)] Department of Civil, Environmental and Architectural Engineering, University of Padova, via Marzolo 9 - Padova, 35131, Italy. E-mail: luca.marchi@dicea.unipd.it
[(2)] Department of Civil, Chemical, Environmental and Materials Engineering, University of Bologna, viale Risorgimento 2 - Bologna, 40136, Italy. E-mail: luca.pozza2@unibo.it; francesca.ferretti10@unibo.it

Abstract

High performance dampers are a key component in low-damage earthquake-resistant timber structures and they should be designed according to displacement-based design criteria. In this case, a well-defined non-linear force vs. displacement relationship of the connection is to be known by the designer (e.g., to evaluate inter-storey drifts), underlying the importance of their careful experimental characterization. In this study, the cyclic shear response of a panel-to-panel joint, fastened to the wooden elements with three alternative solutions, was experimentally tested. Results showed that, although fulfilling the capacity design criteria and allowing an easy replacement of the damper, the semi-rigid nature of fastenings produces important modifications to the mechanical properties of the whole connection type, such as elastic stiffness, yielding point, ductility and equivalent viscous damping.

Keywords: steel damper; timber structures; cross-laminated timber; low-damage structures, seismic design; experimental tests.

1. Introduction

The use of Cross Laminated Timber (CLT) panels has become particularly popular in the field of earthquake-resistant multi-storey structures. The combination of massive panels, post-tensioned systems and dampers allows the realisation of massive seismic-force resisting systems when employed as shear-resisting rocking walls [1,2]. However, the fragile nature of timber demands that energy dissipation capacity is exclusively concentrated into the connections, either with the foundation [3] or between adjacent panels/columns [4]. Therefore, the employment of high-performance dampers is of utmost importance in these structures. Additionally, as these systems are to be designed with the displacement-based design and, more recently, with low-damage concepts [5, 6], the determination of the real mechanical performance of the dampers is again critical. In this context, the designer must have knowledge of the exact non-linear force vs. displacement relationship to predict actual inter-storey uplifts and drifts and to properly design the whole shear wall system. Furthermore, low-damage systems are considered the next generation of structures realised with mass timber panels [7]. Thus, the connection of the damper must undergo very limited to no damage at all in order to provide an easy replaceability of the fuse after the development of irreversible deformations due to high-intensity seismic shocks [8].
Concerning the new generation of dissipative devices for CLT structures, prototypes and commercialised products have been experimentally tested to analyse their non-linear hysteretic response and to validate actual and new methodologies for their design. As a consequence of the great effort provided by the scientific community in studying these novel systems, the ongoing revision of Chapter 8 of Eurocode 8 [9] has opened to the possibility of using purposely developed energy dissipation dampers to design future earthquake-resistant timber structures.
The mechanical characterization and efficiency of a dissipative connection have to be evaluated experimentally by testing:

- the sole dissipating element;
- the dissipating element and its fastening to the CLT panel;
- the dissipating element as part of an entire shear wall system, adopting one or multiple devices [4].

In general, to provide adequate evidence of the behaviour of a dissipating system, there is no need to follow this three-step experimental procedure. Actually, in several cases, at least one step is substituted with alternative numerical or analytical tools [10, 11].

The term "connection" or "connection type" indicates an assembly of different components: the damper itself and the elements used to anchor it to the CLT panel. To this aim, the Eurocode 8 revision [9] provides clear recommendations regarding the application of the capacity design criteria at all levels. Concerning connections, the adopted methodology exploits the force-based design to ensure that components that may be subjected to brittle failures are oversized by including a specific overstrength factor to be applied to the fragile element, evaluated case-by-case. Conversely, the requirement of stiffness does not need to be demonstrated by the less-ductile element of the connection [9]. This clashes with the fact that most of the innovative dampers, such as steel fuses and frictional devices, present a high elastic stiffness and develop all their displacement capacity in the post-yielding phase. Moreover, connections of dampers are still realised with traditional fasteners (mostly dowel-type fasteners), which are known for being considered as semi-rigid joints. Therefore, the elements connecting the damper to the CLT panel (i.e., the brittle component of the connection) must be characterized by a limited displacement capacity in addition to the overstrength requirement.

Although analytical models have been recently developed to calculate strength and stiffness of the most common fasteners for CLT [12], there is a lack of experimental evidence on how the different fastenings for dissipating elements may affect the overall dissipative performance. Very few studies reported experimental tests supported by design procedures to evaluate the performance of the whole connection types in terms of both strength and stiffness or displacement capacity.

In this context, it is likely that the performances of traditional dowel-type fasteners, such as nails, screws and dowels, even when designed in fulfilment of the capacity design criteria, do not allow the full exploitation of the hysteretic response of the damper and strengthening methods have been therefore investigated in the literature.

Pioneering works about strengthening and stiffening of dowelled connections were performed using injection of resins in proximity of the holes [13], applying external toothed metal plates to share embedment between steel and timber [14], or reducing installation gaps with expanded steel tubes [15]. More recently, CFRP (Carbon Fiber Reinforced Polymer) laminates and GFRP (Glass Fiber Reinforced Polymer) fabrics were investigated as local strengthening of traditional dowels [11, 16, 17] and large diameter tubes [18]. Lately, local strengthening to avoid shear plug failure was explored by gluing a squared steel plate with polyurethane adhesive [14].

An alternative to surface coatings is to increase the contact area by using large diameter fasteners. Eurocode 5 [19] sets a limit to the validity of the rules for dowels, equal to 30 mm for the nominal diameter, whereas larger circular connectors are intended as split rings or shear connectors complying with EN 912 [20], i.e., having a nominal diameter larger than 65 mm and a penetration depth equal or less than 30 mm. Experimental tests available in the literature with dowel-type fasteners larger than 30 mm are very limited [21–23]. The overall concept of this method is to spread the localised stress causing wood embedment to a wider surface while preventing the brittle failures that occur due to the concurring peak tensile stresses that develop in the weakest direction, i.e., orthogonal to the grain.

A third alternative solution exploits the use of metal inserts [16] which allows the use of traditional diameter fasteners. In comparison to shear connectors, they provide a pass-through installation which requires the drilling of a large diameter hole throughout the entire thickness of the timber member.

This paper studied how the different fastenings of an elastoplastic steel damper affects the overall hysteretic response of a shear connection between CLT panels. In detail, the study analysed three different fastenings: a) a steel plate fastened with traditional annular ringed nails; b) the same nailed steel plate reinforced with a carbon fabric glued with epoxy resin, installed prior to the nailing of the plate; c) circular large-diameter plastic bushing, reinforced with self-tapping screws. The first solution represents a simple technique in which many small-diameter fasteners are used. Capacity design criteria and load bearing capacity, according to current codes, were used to design it. The second method represents a strengthening method to be applied on connections involving only the outer layers of the CLT panel. The carbon textile aims to ensure a higher strength and stiffness to the connection. The third methodology involves large diameter plastic bushings that engages several layers of the CLT panels. The method explores new opportunities given by extruded

polyamides (a recyclable material), whose mechanical properties can be adjusted according to the allowable elastic deformation to be applied at the joint, e.g., by adding a percentage of filling to the plastic compound.
The overall goal of the present study was to provide experimental evidence on how the performance of a damper for earthquake resistant CLT structures is affected by an over-resistant anchoring system, designed according to capacity design rules but having different stiffness/displacement capacity. Main mechanical parameters such as maximum resistance, elastic and post-elastic stiffness, dissipated energy and viscous damping ratio were extrapolated from each test. Finally, comparisons between experimental and analytical design methods according to available standards were considered.

2. Experimental Campaign

To investigate the influence of the fastenings on the global cyclic response of a panel-to-panel joint, an experimental campaign involving twelve different cyclic tests on full-scale assemblies of CLT panels was performed at the laboratory of the University of Bologna (Italy). Specimen characteristics, test setup and loading protocol are presented in the following.

2.1. Experimental program

The test campaign aimed to test three different fastenings for the same X-bracket steel damper designed for CLT structures: (a) nailed plate, (b) nailed plate reinforced with carbon fabric and (c) screwed plastic inserts (named *bushings* from now on). The direction of the outer layer of boards (either 0° or 90°) with respect to the main loading direction was also included as an additional variable. To assess the performance of these fastening types in low-damage systems, each fastening was tested by executing two consequent fully cyclic loading protocols on the same specimens, in which the steel dampers only were substituted between the first and the second test run. The specimen characteristics and their identification are summarised in Table 1. To provide a clearer comparison (see Section 4), one additional test was included in the set: it was performed in previous research by the authors [8] on a damper rigidly fastened to a steel frame by means of M16 8.8-class steel bolts. This configuration is implicitly assumed to be equivalent to an infinitely stiff connection of the damper to the CLT panel and will be referred to as “rigid” in the following.

Table 1 Characteristics of the specimens

Specimen ID	Connection type	Fasteners per CLT side	Direction of external layer of CLT panel	N° of dampers per test	N° of test run
Rigid	Bolted to a steel frame	-	-	1	1
NP_0	Nailed steel plate	40 nails 4 x 60 mm	Parallel to the edge	4	2
NP_90			Perpendicular to the edge	4	2
RNP_0	Nailed steel plate with carbon fabric	40 nails 4 x 60 mm	Parallel to the edge	4	2
RNP_90			Perpendicular to the edge	4	2
SB_0	Screwed Plastic bushings	4 screws 10 x 350 mm	Parallel to the edge	4	2
SB_90			Perpendicular to the edge	4	2

2.2. General material properties

The forty-eight X-bracket dampers used in the experimental tests were produced by laser cutting an 8-mm thick steel plate with grade equal to S355 [24]. Further details of the employed X-bracket dampers, denoted here simply as dampers, are available in [8, 25] .
Each timber panel was realised by flatwise gluing a pair of 5 crosswise laminated board layers CLT panels, providing a total thickness of 200 mm. The grade of the single boards was C24 according to [26], while the panels were characterised according to their homologation document [27]. The density of the panel, evaluated according to EN 384 [28], was equal to 432 kg/m^3.

2.3. Fastenings

The first fastening type (Fig. 1), hereafter referred to as **Nail Plate (NP) fastening**, adopted a pair of 6-mm thick steel plates per damper with an outer dimension of 120 x 430 mm² realised with S275 steel [24]. The plates, placed in specific milled slots, having a depth of 6 mm and realised on the outer layer of the timber panels, were fastened with 40 annular ringed nails with dimensions of 4 × 60 mm [29]. Nails were distributed on four rows with spacing complying with Eurocode 5 [19]. The yielding moment of the nails was evaluated according to EN 409 [30], obtaining an average value of 8282 N·mm. The damper was fastened to the plate with 16-mm 8.8-class pass-through threaded bars using two nuts at each bar end. The plate was reinforced in proximity to each hole, by welding a 50 x 50 mm square plate, 8-mm thick, to prevent steel embedment.

The second fastening type, henceforth denoted as **Reinforced Nail Plate (RNP) fastening**, exploited the same connection of the NP fastening, apart from the fact that in this case the surface of the milling in the outer layer of the panel was strengthened with a multiaxial carbon fabric glued with epoxy resin. Then, without any additional adhesives or primers, the steel plate was nailed to the timber. The employed fabric had a density of 400 g·m^{-2}, a dry fibre tensile strength of 3000 MPa and an elastic modulus of 240 GPa. Additional mechanical properties of this strengthening method, e.g., bond properties experimentally determined, are available in [11].

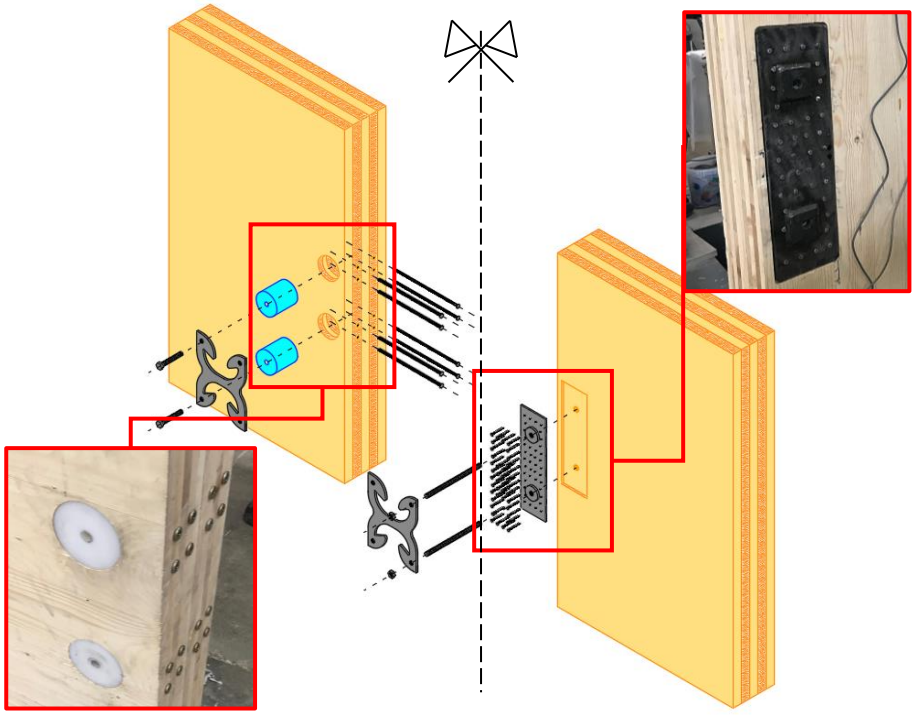

Fig. 1. X-bracket damper attachment with nailed plate NP connections (right) or screwed plastic bushings SB (left).

The last fastening type, named **Screwed Bushing (SB) fastening** from now on, consisted in the realisation of a pair of 100-mm circular holes in the CLT panel, one for each fastening point of the damper, in which nylon-based large-diameter bushings were inserted (Fig. 1). These holes were CNC-machined by the manufacturer of the CLT specimens. The plastic bushings were cut from a 100-mm diameter extruded cylindrical profile of unreinforced Polyamide 6, having a density of 1150 kg/m^3. Each bushing, with dimensions 100 x 100 mm, was provided with a 16-mm pass-through hole to accommodate the 8.8 strength-class steel bolts, with dimensions of 16 x 280 mm, that secured the damper to the panel.

Given the fixed spacing between the holes of the damper, the edge spacing of the bushings was set equal to 77 mm. Eurocode 5 [19] does not consider dowel-type fasteners having a diameter greater than 30 mm, but it provides rules for split rings and shear plate connectors: depending on the loading direction and the orientation of the external layer of boards with respect to the edge, the minimum edge distance varies between 0.6ϕ (unloaded edge) and 2ϕ (loaded end), where ϕ is the diameter of the connectors. Consequently, to avoid anticipated shear plug failures, the bushings were fastened to the timber panel with two full-threaded

self-tapping screws with dimensions of 10 × 350 mm. The pair of screws, inserted edgewise in the panel, were threaded on the first available layer of board parallel to the edge, excluding the outer layer. Predrilling with an 8-mm drill bit was performed up to a depth of 100 mm to include the partial predrilling of the plastic bushing.

2.4. Full specimen characteristics and test setup

Tests were performed with a doubly symmetric setup in which two lateral CLT elements, with dimension equal to 1200 mm x 1480 mm (B x H), were connected by means of four dampers (two for each face) to a central CLT element having dimensions of 740 mm x 900 mm (Fig. 2). The two lateral panels were equipped with a notch on each end to house the termination plates of the Dywidag threadbar anchors, necessary to rigidly connect the panels to the strong floor and to prevent their rocking during the cyclic tests. The central CLT element was enclosed into a steel frame composed by steel profiles and four Dywidag anchors, rigidly attached to a servo-hydraulic actuator. All Dywidag anchors, having a nominal diameter equal to 30 mm, were pretensioned to prevent any gap opening at the base of the lateral elements and between the upper edge of the central panel and the jack. Such pretension allowed contrasting the out-of-plane displacements of the whole assembled specimen. However, four additional steel plates, nailed to the edges of the central panel, were added to further restrain the out-of-plane displacements between lateral and central panels. Teflon pads were added between the restraining plates and the CLT surfaces to avoid development of parasite frictional forces.

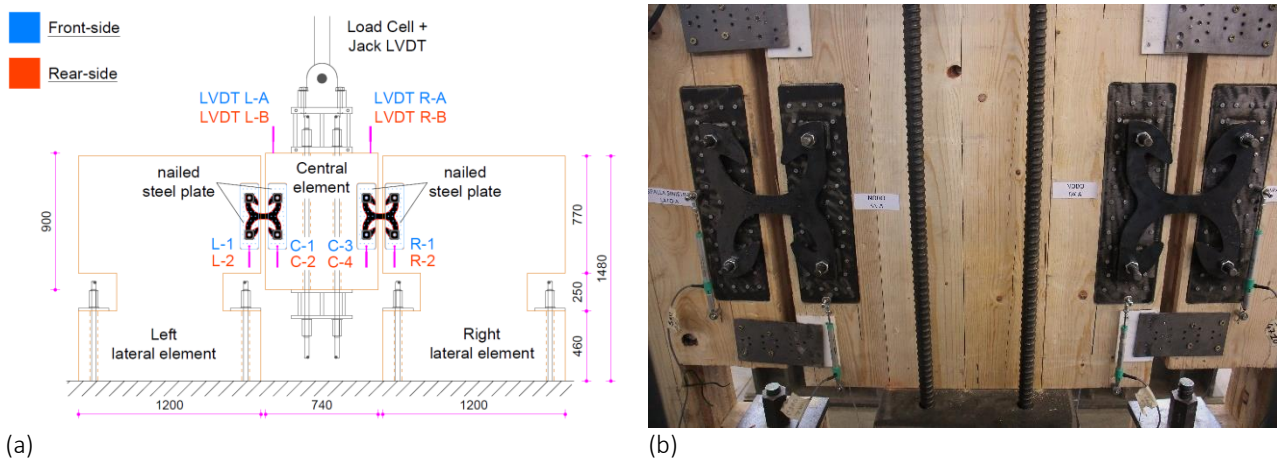

Fig. 2. Setup geometry (a) and instrument disposition (b) for NP and RNP fastenings.

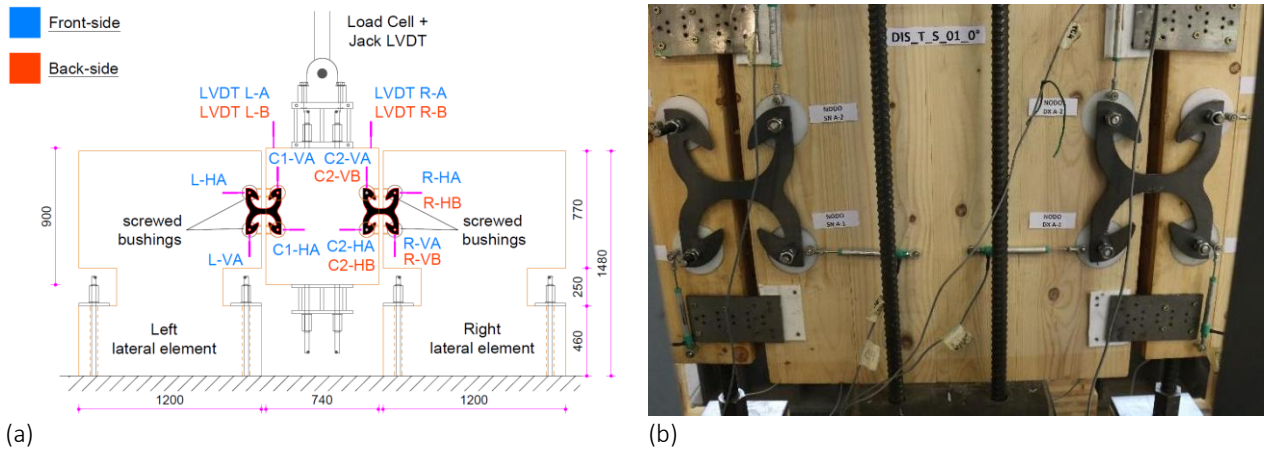

Fig. 3. Setup geometry (a) and instrument disposition (b) for SB fastening.

A single load cell (500kN of rated load capacity) was used to measure the load applied to the central panel. The relative displacement between the three panels was monitored by four Linear Variable Differential Transducers (LVDTs) (L-A, L-B, R-A and R-B in Fig. 2a and Fig. 3a), placed symmetrically on the upper edge of the specimens, each one measuring the uplift of one corner of the central panel. The relative vertical slip between the connection of the damper and the CLT panel was recorded through eight potentiometers, i.e., a

pair per damper (Fig. 2b). For the SB fastening, each damper and its connection were monitored with four potentiometers: two potentiometers measured the vertical slip, as for the other fastening types, while two potentiometers were positioned horizontally to monitor the slip of the bushing occurring in the direction orthogonal to the edge (Fig. 3b). Each channel was recorded simultaneously with a datalogger at a constant frequency of 1 Hz.

2.5. Load protocol and yielding displacement evaluation

The reference for the displacement-controlled cyclic load protocol, according to EN 12512 [31], was set to be the overall panel-to-panel shear slip. The estimated yielding displacement $d_{y,est}$, taken as reference for the definition of the load protocol, was derived starting from the experimental response of the sole damper, available from a previous work by the authors [8]. As introduced in Section 2.1, in those tests, the damper was rigidly fastened to a steel frame and cyclically loaded in shear, leading to a value of d_y equal to 4 mm. An infinite stiffness of the connection between the damper and the CLT panel was implicitly assumed. Such value was also confirmed in detailed numerical simulations involving the same type of damper [25]. In this campaign, the additional slip due to the deformability of the connections was also considered. As an example, for the NP fastening, an extra displacement of 1 mm was assumed (i.e. the nail gap), then setting an overall $d_{y,est}$ value of 5 mm, a yielding force of 40 kN and an elastic stiffness k_{ser} of 0.93 kN/mm per nail according to [11]. To provide coherent comparisons in the analysis, the same value of $d_{y,est}$ was assumed for all the three investigated fastenings.
Cyclic tests were carried out performing a single cycle repetition up to 25% and 50% of $d_{y,est}$ and three cycles repetitions at 75%, 100%, 200%, 400%, 600% and 800% of this value. The highest target displacements were not reached in all the tests, as will be explained in the following. Tests were performed under displacement control, adopting a displacement rate of 0.04 mm/s during the cycles, then increased to a maximum value of 0.3 mm/s during the final loading phase (up to failure of the connection).

3. Experimental Results

This section describes the experimental outcomes in terms of failure modes, force-displacement curves of the panel-to-panel joint and relative displacements measured for each of the three fastening types.

3.1. Failure modes and residual damages

In each of the twelve cyclic tests, the yielding of all four dampers was activated, achieving inelastic deformations of the steel elements and registering large slips at the panel-to-panel interface. Coherent with previous tests on similar types of dampers [32], the failure occurred in the zones where a concentration of plastic strains mostly occurred, namely in the transition between the horizontal arms and the vertical web of the X-bracket steel damper, as representatively shown in Fig. 4 for the different fastenings. The cyclic loading procedure was interrupted by the first rupture of one of the four dampers.
For each configuration, once the two test runs were completed, all the dampers, connections and panels were disassembled and carefully inspected. The residual deformation observed in the nailed plate configuration (NP_90) are shown in Fig. 5a. The row of nails in proximity to the plate ends exhibited a combination of yielding of steel and wood embedment, determining a limited but visible slip. Such deformations did not occur in any of the RNP joints (Fig. 5b), confirming that the composite fabric prevented local damages of the wooden layer close to the nails. In RNP joints, the panel surface was intact and the nails did not show any plastic hinges, differently from what were observed in the NP joints. In SB joints, the plastic bushings showed no damages in any of the specimens, and the bushing-to-panel interface was intact (Fig. 5c). The first millimetres of the threaded holes of the bushings were characterised by minor irreversible deformations which caused a partial rotation of the bolts at high displacement values. The bushings were removed and flipped after the first test run. Also, the self-tapping screws securing the plastic bushings were undamaged and could be unscrewed easily after the tests. Additionally, no crack opening on the timber panels was observed in all the fastening configurations.

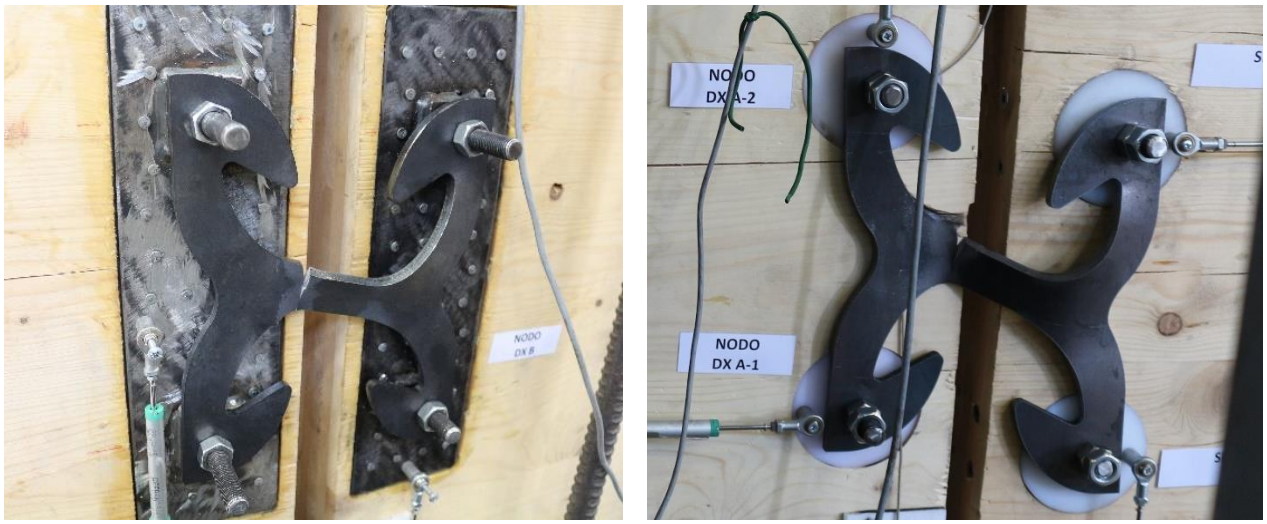

(a) (b)

Fig. 4. Failure modes of the dampers for (a) NP and RNP fastenings and (b) SB fastening.

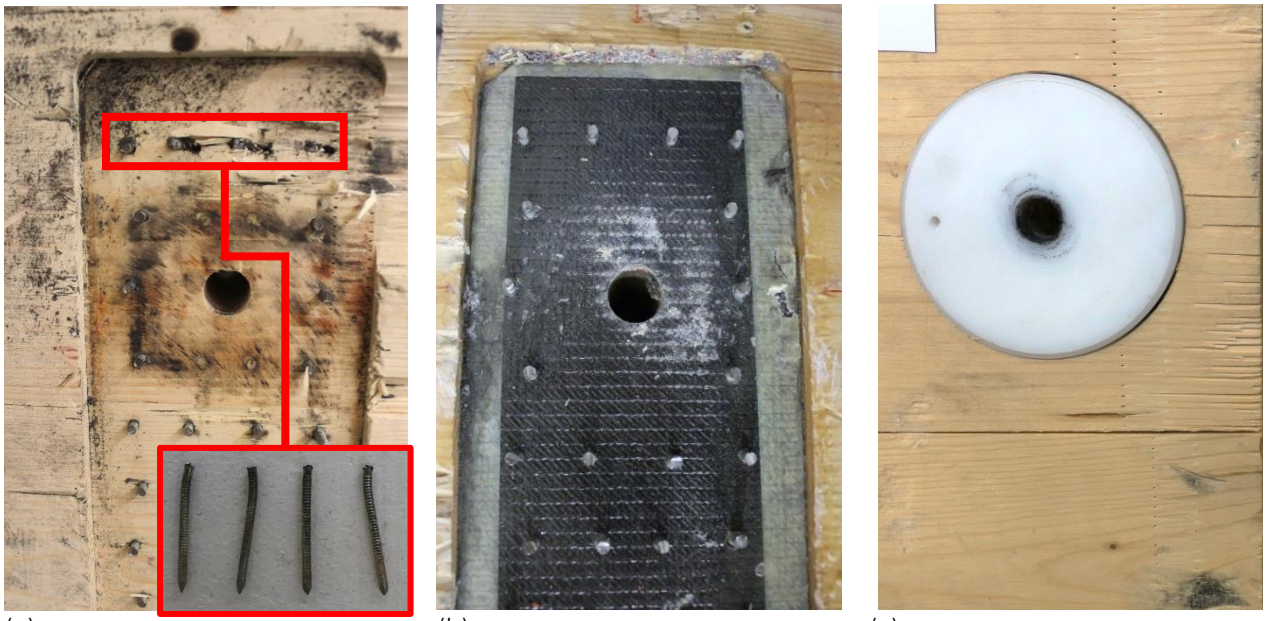

(a) (b) (c)

Fig. 5. Residual damages after two test runs on the three fastening types: NP_90 (a), RNP_90 (b) and SB_90 (c).

3.2. Global response of the connection

The overall cyclic response of each fastening was described by averaged force-displacement loops (see Fig. 6 in which curves for the first test run are reported); in more detail, displacements (δ_t) were derived by averaging the signals of the four LVDTs measuring the relative slip between the panels, while the force was obtained by dividing the total applied load by four, i.e., assuming an equivalent distribution of the forces among all the dampers.

The loops provided evidence of the cyclic response of a connection composed by elements with different hysteretic responses working in series. In this case, the force applied by the actuator was transmitted to the fastening on the central panel, then to the dampers, and finally to the fastenings of the lateral panels. The flux of forces was influenced by the presence of elements with different hysteretic responses producing a global behaviour that was a combination of the single elements working in series. Therefore, the global response showed large inelastic deformations and dissipated energy (provided by the steel fuse), but it was also characterised by a pinching phenomenon, since the connection to the panel was not able to provide an infinitely stiff behaviour, thus determining a modification in the global panel-to-panel joint response.

In general, it appeared that the different type of fastenings affected the capacity of the whole connection assembly, both in terms of maximum load reached for each cycle and ultimate displacement capacity. In particular, NP specimens completed all the three cycles at a displacement up to ±20 mm (4 × $d_{y,est}$). The first test with the load parallel to the grain joint (NP_0-1) stopped after the 2nd cycle at an amplitude of ±30 mm (6 × $d_{y,est}$), but the second test run (NP_0-2) reached the failure of the damper just after the first ramp up to 30 mm. NP_90-1 completed all the cycles at ±30 mm, but again the second test run (NP_90-2) failed during the first ramp of the 30-mm amplitude cycles. RNP fastening provided a more stable behaviour by completing all the cycles up to ±30 mm (6 × $d_{y,est}$) and failing in the first ramp up to the 40-mm amplitude cycle (8 × $d_{y,est}$). Tests with SB fastening behaved similarly to the RNP joint, and also completed the first cycle at a displacement level of ±40 mm before failure of the dampers took place.

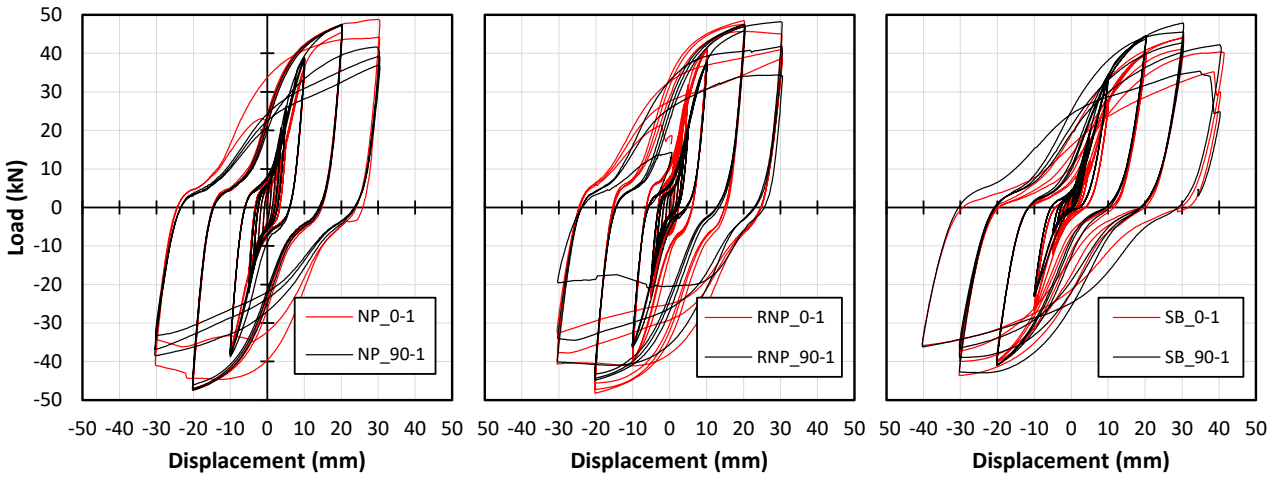

Fig. 6 Panel-to-panel load-displacement loops for the first test run for different grain orientation of the outer layer respect to the load direction.

3.3. First and second test runs

All the three fastening types were characterized by negligible damages after the first of the two subsequent test runs. Removal of the steel rods and substitution of the dampers resulted in a straightforward operation once the central CLT panel was aligned back to the initial position. For NP and RNP fastenings, the pass-through threaded rods showed no damage, however new bars were provided after each test. Bolts in SB joints exhibited some limited yielding and were substituted as well.

For all the three fastening types, the hysteretic loop of the second test run approximately overlapped the first one (Fig. 7). A slight increase of the pinching phenomenon in the second test run (i.e., a reduction of the reloading stiffness) was registered in all cases, with no degradation of the resistance. Small differences observed comparing first and second test runs could also be related to an intrinsic variability of the whole connection and to the hysteretic response of the dampers. It must be highlighted that none of the connections showed the transition to a post-elastic response or any sudden drops of resistance, therefore fulfilling the capacity design criteria under which the connections were designed.

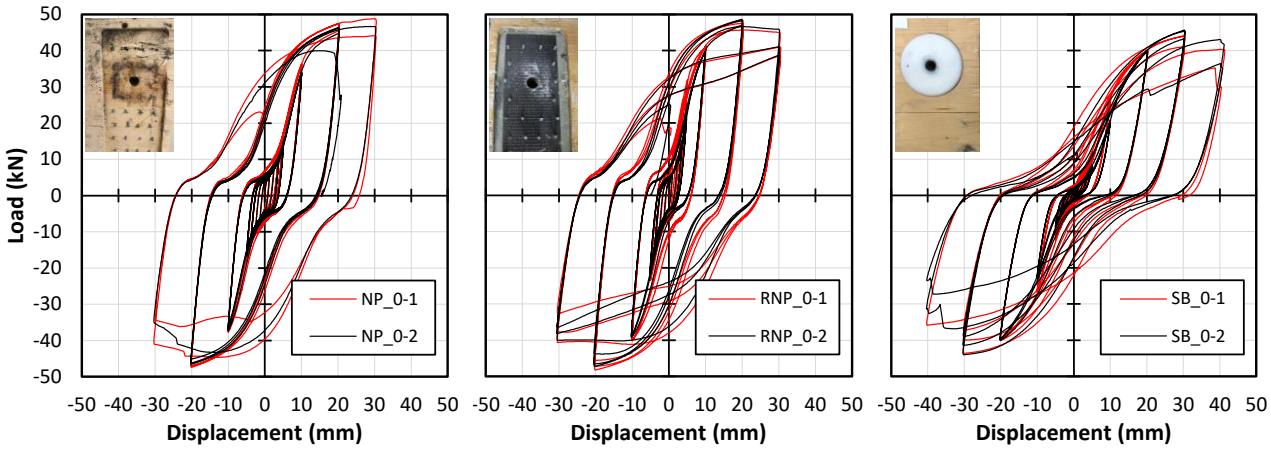

Fig. 7. Load-Displacement curves between first and second test run for the different fastening types in the 0° configuration.

3.4. Local response of fastenings

To decouple the cyclic response of the fastening from the one of the whole connection, the load-displacement curves of each element connecting the damper were obtained from the data recorded by the potentiometers. For each damper, the sum of the vertical slips registered between panel and connection for both the central and the lateral panels were used to plot the net load-displacements curves in Fig. 8, in which results for the first test runs are reported.

The NP fastening returned a hysteretic response typical of small-diameter dowel-type fasteners, characterised by an evident pinching phenomenon and peak displacements up to ±1.4 mm and ±1.6 mm on specimens loaded parallel and perpendicular to the grain, respectively. The addition of the carbon fabric reinforcement (RNP fastening) led to a reduction of the peak displacements for subsequent cycles, with values below ±1.0 mm and negligible differences for both grain directions. On the opposite, the SB fastening produced quite different responses between the two grain directions: the most evident pinching phenomenon was registered for the SB_0 configuration (parallel to grain), with a relative displacement up to 3.8 mm, while peak displacements between 1.5-2.5 mm and a pinching almost coincident with the NP connection were observed for the SB_90 joint (perpendicular to grain). This may be attributed to the material elastic modulus which is about three times lower than that of the wood parallel to the grain, but ten times higher than wood orthogonal to the grain. The higher slips may also be due to the presence of gaps between the bushings and the holes in the wooden panels, which may be also responsible for the slightly unsymmetric hysteretic response of the connection that emerged in all tests.

The contribution of the slip of the connection to the overall displacement capacity was expressed as the ratio between the effective connection slip parallel to the loading force δ_c and the total displacement of the panel-to-panel joint δ_t (Fig. 9). Such ratio shows the highest values (up to 25% and 50% for the tests NP_90 and SB_0, respectively) when the dampers still behave elastically. Some slight asymmetry characterised all fastening types as well. With the onset of yielding and the consequent reduction of stiffness at the damper level, the average ratios decreased to the range of 2-10% at the highest displacement amplitudes. Such ratio may be seen as the result of the overall deformability provided by the connection type, which will be detailed in Section 4.2. It is worth noting that the second test run produced always equal or slightly higher displacements than the first test run, except for SB_90 tests.

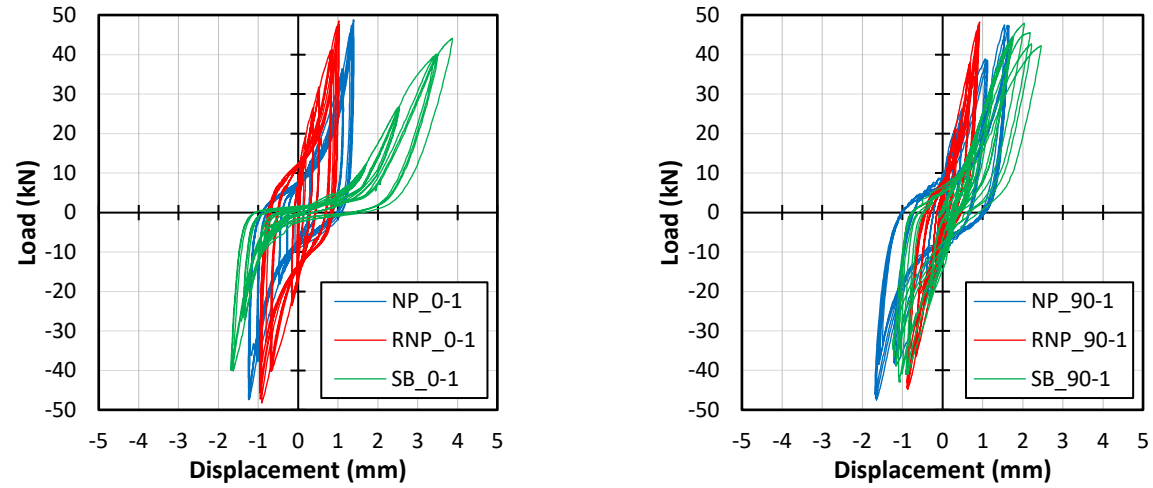

Fig. 8. Load-Displacement curves limited to the slip of the anchoring element of the first test run in the 0° (a) and 90° (b) configurations.

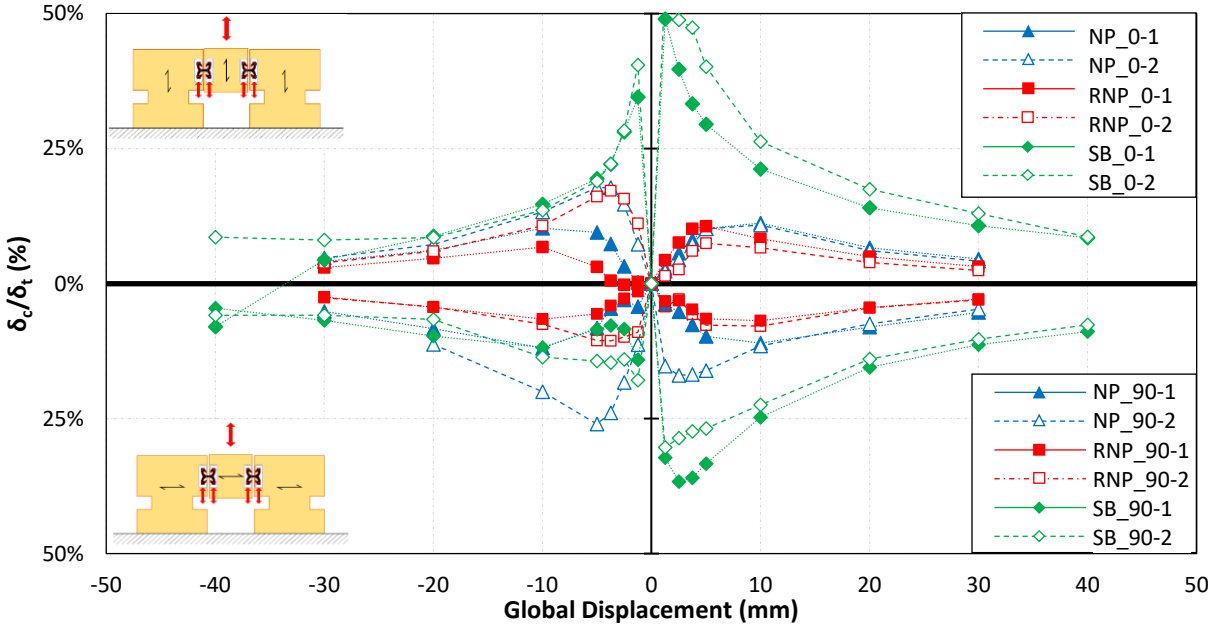

Fig. 9. Comparison of average effective connection slip and global slip for all the fastening types at significant drift levels for load parallel and perpendicular to grain direction.

4. Analysis of results and discussion

This section reports the calculation and the comparisons of the main mechanical parameters for each fastening type through suitable linearization methods.

4.1. Yielding point, stiffness and ductility class

As the ductility capacity is conventionally expressed as the ratio $\mu = d_u/d_y$, it varies according to the specific definition of the yielding displacement d_y and the ultimate displacement d_u and, consequently, to the chosen linearization method [33]. Therefore, the process used to interpret and simplify the non-linear backbone curve of the hysteretic cycle is a crucial point. Several methods have been proposed in the literature to extrapolate the yielding and ultimate conditions of timber connections from experimental tests [33]. In this work, the chosen approach follows a recent proposal for cyclic experimental tests of connections for CLT [34]. Within this method, a trilinear model is adopted, characterized by three distinct branches: (i) the first branch accounts for the possible delayed/anticipated stiffening at the beginning of the loading phase; (ii) the second branch is

defined by the slope K_{el} of the line connecting the points of the experimental curve at 20% and 50% of the maximum force, similarly to the procedure defined by EN12512 [31]; (iii) the third one is defined as the segment passing through the peak-force point (F_{max},d_{Fmax}) with a slope K_p obtained by imposing the strain energy equivalence between the experimental envelope curve and the trilinear approximation. In more detail, the three branches are calculated in the following order: the slope of the second branch is initially defined as explained, then, the first branch is evaluated starting from the origin up to the point (d_{y1},F_{y1}) by considering a stiffness K_i either equal to the average unloading stiffness calculated on the large displacement cycles (Fig. 10a) or determined by connecting the origin and the point of the experimental curve at 20% of F_{max} (Fig. 10b), whether the intercept of the second branch with the horizontal axis is negative or positive, respectively. Finally, after the determination of the slope of the third branch, the second point of the trilinear curve (d_{y2},F_{y2}), i.e., the real yielding point, is defined as the intersection between the second and third branch lines.
With respect to the ultimate condition, the method follows current standard suggestions [9], setting a limit to the ultimate slip of the connection either equal to the slip at failure in case of a hardening behaviour (i.e., $d_u = d_{Fmax}$) or equal to the slip in correspondence with a load drop to the 80% of the maximum force F_{max} if softening occurs (i.e., $d_u > d_{Fmax}$). The new provisions of Eurocode 8 [9] require that the dissipative zones shall be able to deform plastically for at least three fully reversed cycles at their static ductility ratio, without more than a 20% reduction of their resistance between the first and third cycle of the backbone curve. Therefore, the final ductility of the connection is related to the condition of showing some hysteresis at the maximum displacement capacity.

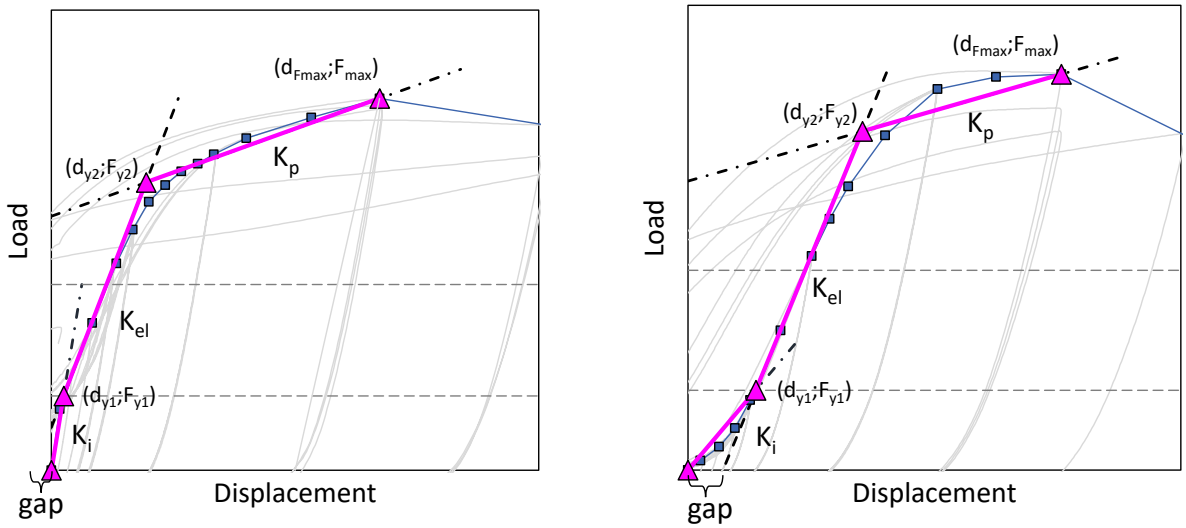

Fig. 10. Trilinear approximation of the load-displacement curves with different initial stiffness K_i (negative (a) or positive (b) intercept of the second branch with the horizontal axis).

The key parameters obtained for all the tests are summarised in Table 2, comprising the results of the damper rigidly fastened to a steel frame. In general, it clearly emerged that all the three fastenings affected the mechanical parameters of the damper. No fastening type could be defined as a lower/upper bound condition, as the results were quite variable according to each investigated parameter. For example, SB specimens provided the lowest elastic stiffness K_{el}, whereas the NP fastening returned the lowest ductility. The delayed response, causing an apparent pinching-like phenomenon, was particularly evident for the SB_0 specimens and less or absent for the nailed configurations, both unreinforced and reinforced.
Referring to the first test run, the yielding displacement d_{y2} showed a considerable shift, up to three times higher than the rigid system for the SB solution (from 4.4 mm to 12.0 mm on average), about twice for the NP fastening and more than 70% for the RNP fastening. On the contrary, the yielding force F_{y2} was always close to the rigid configuration, indicating that the fastenings were over resistant not only in ultimate conditions but at yielding as well, and both yielding and failure were governed by the damper only. Again, taking the rigid configuration as a reference, the elastic stiffness K_{el} was reduced from an average of 7.5 kN/mm down to 4.2, 5.1 and 3.1 kN/mm for the NP, RNP and SB fastenings, respectively. It is worth noting that the stiffness

increment of the RNP solution, quantified approximately as the 70% in the characterization test campaign [11], was reduced to 21% in the overall connection assembly.

According to the provisions of the new revision of the Eurocode 8 [9] regarding the seismic design of timber structures, a connection system for cantilever structures shall provide static ductility value equal to 2.5 or higher. Considering only the first test run, it is visible how the shifting of the yielding displacement d_{y2}, with respect to the rigid configuration, led to unsatisfactory results for the NP fastening, characterized by a ductility equal to 2.2 on average. In the tests involving the RNP solution, the combination of the highest values of K_{el} and the consequent limited shift of the yielding point led to the highest ductility (2.7 on average). In the SB strengthening solution, the highest yielding displacement d_{y2} observed in the set was counterbalanced by an ultimate displacement equal to 30 mm (rather than the 20 mm target observed in most tests) and therefore ductility requirements were satisfied. Such an outcome demonstrates that the use of different fastenings for the same dissipative element would lead to different ductility classes and, therefore, to important implications with respect to the design of a structure with those elements. This gains even more importance considering that the current capacity design criteria on all three fastening types are fulfilled.

It is worth noting that, for all the three fastenings, a shift of the yielding displacement d_{y2}, approximately equal to 1.0-1.4 mm, was noticed in the second test run. However, no noteworthy modifications of the elastic stiffness K_{el} were observed (-5% on average between all the tested configurations). This phenomenon affects the average static ductility, which is characterized by a decrease, calculated between 0.2 and 0.4 (-10% on average between all the tested configurations). Therefore, by performing subsequent tests on the same fastening methods it is possible to thoroughly predict their contribution to the global response of the connection system.

Table 2 Yielding point, elastic stiffness and ductility according to the linearization method.

Specimen ID		d_{y1} (mm)	F_{y1} (kN)	d_{y2} (mm)	F_{y2} (kN)	d_{Fmax} (mm)	F_{max} (kN)	K_{el} (kN/mm)	K_p (kN/mm)	μ (-)	Gap (mm)	K_i (kN/mm)
Rigid	+	1.1	9.7	4.4	34.8	19.9	48.3	7.6	0.9	4.5	-0.2	8.8
	-	1.1	9.7	4.7	36.8	20.2	48.5	7.5	0.8	4.3	-0.3	9.2
NP_0-1	+	3.1	9.8	9.9	38.2	20.2	47.5	4.2	1.0	2.0	0.8	3.1
	-	2.6	9.5	10.2	38.7	20.2	47.5	3.8	0.9	2.0	0.1	3.6
NP_90-1	+	1.3	9.6	7.4	37.1	20.2	47.4	4.5	0.9	2.7	-0.8	7.4
	-	2.0	9.5	9.1	39.4	20.2	47.4	4.2	0.7	2.2	-0.3	4.7
Avg.		**2.3**	**9.6**	**9.2**	**38.3**	**20.2**	**47.5**	**4.2**	**0.9**	**2.2**	**-0.1**	**4.7**
NP_0-2	+	3.3	9.3	11.5	39.7	20.2	46.5	3.7	0.8	1.7	0.8	2.8
	-	2.6	9.3	11.6	41.4	20.2	46.5	3.6	0.6	1.7	0.0	3.6
NP_90-2	+	1.4	9.2	7.6	36.4	20.2	46.0	4.4	0.8	2.7	-0.8	6.8
	-	2.1	9.8	10.1	43.3	20.0	49.1	4.2	0.6	2.0	-0.2	4.7
Avg.		**2.3**	**9.4**	**10.2**	**40.2**	**20.2**	**47.0**	**4.0**	**0.7**	**2.0**	**-0.1**	**4.5**
RNP_0-1	+	0.8	9.7	5.8	37.6	20.2	48.5	5.5	0.8	3.5	-1.0	12.9
	-	0.0	9.6	8.0	39.1	20.2	48.2	5.0	0.7	2.5	0.2	4.6
RNP_90-1	+	2.9	9.5	7.9	36.7	20.3	47.6	5.5	0.9	2.6	1.2	3.3
	-	0.0	9.0	9.0	36.6	20.2	44.8	4.3	0.7	2.3	0.5	3.4
Avg.		**0.9**	**9.5**	**7.7**	**37.5**	**20.2**	**47.3**	**5.1**	**0.8**	**2.7**	**0.2**	**6.1**
RNP_0-2	+	2.4	9.7	7.7	38.2	20.1	48.5	5.4	0.8	2.6	0.6	4.1
	-	0.0	9.4	9.2	40.1	20.4	47.2	4.4	0.6	2.2	0.0	4.3
RNP_90-2	+	3.3	9.6	10.6	38.4	20.3	47.6	3.9	1.0	1.9	0.9	2.9
	-	0.0	9.0	8.1	36.8	20.2	45.0	4.2	0.7	2.5	-0.5	5.7
Avg.		**1.4**	**9.4**	**8.9**	**38.4**	**20.2**	**47.1**	**4.5**	**0.8**	**2.3**	**0.2**	**4.2**
SB_0-1	+	3.8	8.8	13.6	36.5	30.3	44.0	2.8	0.5	2.2	0.7	2.3
	-	0.0	8.7	12.5	35.0	30.3	43.6	2.9	0.5	2.4	0.5	2.5
SB_90-1	+	2.3	9.6	10.4	38.7	30.3	48.0	3.6	0.5	2.9	-0.4	4.2
	-	0.0	8.6	11.3	36.5	30.3	42.6	3.2	0.4	2.7	2.8	1.6
Avg.		**1.5**	**8.9**	**12.0**	**36.7**	**30.3**	**44.6**	**3.1**	**0.5**	**2.6**	**0.9**	**2.6**
SB_0-2	+	5.5	9.1	15.4	36.3	30.3	45.5	2.7	0.6	2.0	2.2	1.7
	-	4.8	8.8	14.8	39.8	30.3	44.1	2.7	0.3	2.1	1.5	1.8
SB_90-2	+	2.3	9.5	9.3	34.4	30.3	47.5	3.6	0.6	3.3	-0.4	4.1
	-	0.0	9.2	13.9	38.1	30.3	45.7	2.9	0.5	2.2	0.9	2.3
Avg.		**3.2**	**9.1**	**13.3**	**37.1**	**30.3**	**45.7**	**3.0**	**0.5**	**2.4**	**1.1**	**2.5**

Experimental outcomes for the elastic stiffness were compared to the following analytical predictions based on models available in current codes and standards. The panel-to-panel connection was assumed as a system of in series elastic springs, for which the global elastic stiffness $K_{el,th}$ can be calculated starting from the elastic stiffness of each contributing element $K_{ser,i}$ according to Eq. (1):

$$K_{el,th} = \frac{1}{\sum_i \frac{1}{K_{ser,i}}} = \frac{1}{\frac{1}{K_{ser,c}} + \frac{1}{K_{ser,d}} + \frac{1}{K_{ser,c}}} \quad (1)$$

with $K_{ser,d}$ and $K_{ser,c}$ being the elastic stiffness of the damper, corresponding to the average value of K_{el} for the rigid connection (Table 2), and of the anchoring element, respectively. For the NP fastening, the elastic stiffness can be derived from the formulation reported in Eurocode 5 [19] considering the density of wood ρ, the nominal diameter ϕ and number of fasteners n, according to Eq.(2):

$$K_{ser,c} = n \cdot \rho^{1.5} \cdot \phi^{0.8}/30 \quad (2)$$

The stiffening contribution of the textile fabric adopted in RNP connections, shall be calculated on the basis of the experimental tests conducted to characterise the reinforcing method [11]. Here, the authors proposed a method which relies on Eq.(2), adopting an improved density value $\rho = \rho_{mod}$ to account for the different layers of the strengthened surface, according to Eq. (3):

$$\rho_{mod} = \frac{(\rho_t \cdot s_t + \rho_e \cdot s_e + \rho_{CLT} \cdot s_{CLT})}{(s_t + s_e + s_{CLT})} \quad (3)$$

where ρ_t, ρ_e and ρ_{CLT} are, respectively, the dry carbon fabric density, the adhesive density, and the mean density of the CLT layer over which the wood embedment phenomenon was localised; s_t, s_e and s_{CLT} are the respective thicknesses of the three layers.

For the SB fastening, even if these joints are apparently very different from the traditional connections, they were assumed to behave as a large split ring connector with the same large contact interface, for which their stiffness $K_{ser,sb}$ following Eq. (4) proposed in Eurocode 5 [19] can be used:

$$K_{ser,c} = n \cdot K_{ser,sb} = n \cdot \rho \cdot \phi_c/2 \quad (4)$$

where ϕ_c is the connector diameter. For NP and RNP fastenings, the steel bolts may be assumed as infinitely rigid steel-to-steel elements while for SB joints, given the low elastic modulus of the plastic bushing, they should be included in the summation of Eq. (6) as semi-rigid fasteners. In this case, their stiffness $K_{ser,bolts}$ were approximated according to Eurocode 5 [19]:

$$K_{ser,bolts} = n \cdot \rho^{1.5} \cdot \phi_b/23 \quad (5)$$

where ρ_{PA6} is the density of the material used for the bushings and ϕ_b is their external diameter. Therefore, for the SB connections, Eq. (1) shall be rewritten as:

$$K_{ser,th} = \frac{1}{\frac{1}{K_{ser,sb}} + \frac{1}{K_{ser,bolt}} + \frac{1}{K_{ser,d}} + \frac{1}{K_{ser,bolt}} + \frac{1}{K_{ser,sb}}} \quad (6)$$

The assumed parameters and the calculated stiffness values are reported in Table 3, together with the experimental result $K_{el,exp}$, obtained in the first test runs. In general, the analytical results overestimated (+21% on average) the experimental ones, but they correctly captured the trend of the stiffness reduction expected for the fastenings. In more detail, the addition of the semi-rigid behaviour of the steel bolts for SB joints determined the lowest analytical stiffness among the three fastening types, matching the actual trend of the tests. The quantified decrease of stiffness due to the semi-rigid fastening was expressed as the ratio η_k between the elastic stiffness of the different anchoring types and $K_{ser,d}$, and it varied between 39 and 63%, and between 49 and 83% for experimental and analytical values, respectively. The analytical expression matched quite well the experimental values, providing a demonstration of the chain-like behaviour of the connections working in series.

Table 3. Comparison between experimental and analytical elastic stiffness.

Parameter	Units	NP fastening	RNP fastening	SB fastening
ρ_w	kg/m³	402	723*	402
ρ_{PA6}	kg/m³	-	-	1150
ϕ or ϕ_c	mm	4	4	100
n	-	40	40	2
ϕ_b	mm	16	16	16
$K_{ser,c}$ *(Eq. 2)*	kN/mm	34.79	78.64	42.00
$K_{ser,bolts}$ *(Eq. 5)*	kN/mm	-	-	54.26
$K_{ser,d}$	kN/mm	7.50	7.50	7.50
$K_{el,exp.}$	**kN/mm**	**4.18**	**5.08**	**3.13**
$K_{el,th}$ *(Eq.1)*	**kN/mm**	**5.14 (+22.8%)**	**6.27 (+23.5%)**	**3.71 (+18.3%)**
$\eta_{k,exp}$	-	0.56	0.68	0.42
$\eta_{k,th}$	-	0.68	0.84	0.49

* modified according to Eq. (3)

4.2. Force and secant stiffness degradation

Computing the resistance and the secant stiffness degradations (ΔF and ΔK, respectively) obtained in the second and the third loading cycle for significant displacement amplitudes, the analysis of the post-yielding response of the connection was performed. The results obtained are shown in Fig. 11 and Fig. 12 at four displacement amplitudes: 5, 10, 20 and 30 mm, i.e., 1, 2, 4 and 6 times $d_{y,est}$. They are also reported in Table 4. It can be observed that up to 20 mm, all fastenings provided negligible resistance and stiffness degradation, with average values below 5%, except for the second test run, in which values up to 10% were observed for NP and RNP fastenings. It is worth mentioning that, for the tests in which a displacement amplitude of 30 mm was reached, both the force and stiffness degradations were lower in the second test run. The 30-mm displacement amplitude was the threshold at which the unreinforced nailed plate failed to complete the second or third load cycle. The dampers fastened with RNP solution, although fulfilling the three load inversions in all the four tests, manifested a severe strength and stiffness decrease in the third load cycle, with values beyond the 20 % threshold [9]. This mostly occurred in the configuration with load perpendicular to the grain (RNP_90), observing an important difference when direction to the grain is considered. Finally, specimens employing the SB fastening showed the best performance in this context, completing all the cycles and showing limited damages to the system. It is to be recalled that such a solution was capable to provide also a first load inversion up to ±40 mm before failing.

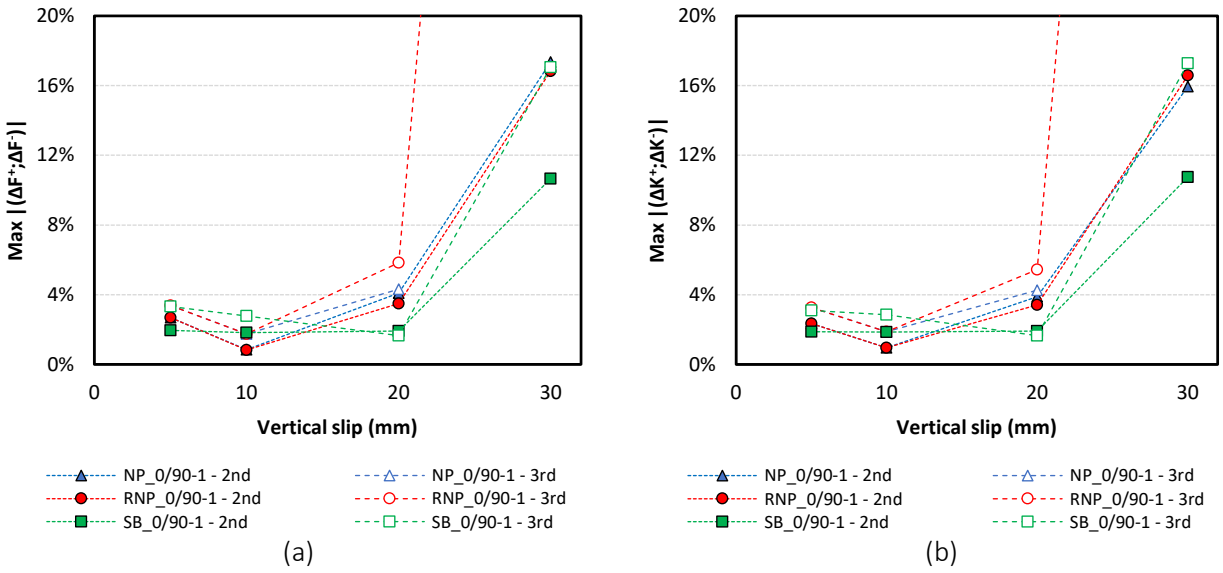

Fig. 11. Force (a) and secant stiffness (b) degradation calculated at significant displacement levels of the second and third loading cycles for the first test run.

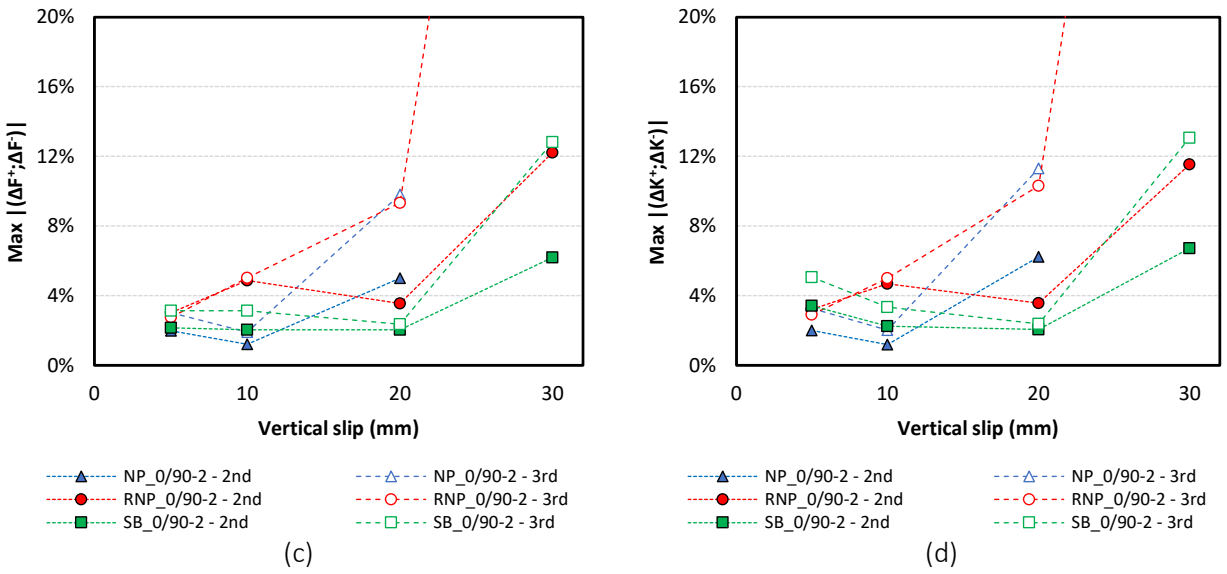

Fig. 12. Force (a) and secant stiffness (b) degradation calculated at significant displacement levels of the second and third loading cycles for the second test run.

Table 4. Force and secant stiffness degradation calculated at 10, 20 and 30 mm of total slip.

		ΔF								ΔK							
		5 mm		10 mm		20 mm		30 mm		5 mm		10 mm		20 mm		30 mm	
		2nd	3rd	2nd	3rd	2nd	3rd	2nd	3rd	2nd	3rd	2nd	3rd	2nd	3rd	2nd	3rd
Rigid	+	0.0%	0.0%	0.0%	0.0%	-0.2%	-5%	0.0%	-11.8%	0.0%	0.0%	0.0%	0.0%	-0.3%	-4.9%	-7.9%	-11.8%
	-	0.0%	0.0%	0.0%	0.0%	0%	-17%	-4.3%	-7.0%	0.0%	0.0%	0.0%	0.0%	-0.5%	-17.4%	-4.3%	-7.0%
NP_0-1	+	-1.3%	-1.6%	-0.1%	-0.4%	4.1%	4.3%	-10.4%	/	-0.9%	-1.4%	-0.3%	-0.7%	3.9%	4.3%	-12.5%	/
	-	-1.5%	-1.6%	-0.8%	-1.3%	0.5%	-0.5%	-17.3%	/	-1.3%	-1.6%	-0.8%	-1.4%	0.5%	-0.2%	-16.0%	/
NP_0-2	+	1.3%	1.1%	0.7%	0.7%	3.5%	3.1%	/	/	1.4%	1.2%	0.7%	0.7%	3.3%	3.2%	/	/
	-	-2.0%	-3.0%	-1.2%	-1.9%	-0.7%	-3.2%	/	/	-2.0%	-2.9%	-1.2%	-2.0%	-0.5%	-2.4%	/	/
NP_90-1	+	-2.7%	-3.4%	-0.5%	-1.3%	-0.3%	-0.6%	-6.3%	-12.8%	-2.3%	-3.3%	-0.5%	-1.6%	0.0%	0.3%	-6.3%	-15.2%
	-	-1.9%	-3.2%	-0.8%	-1.7%	-0.8%	-3.0%	-4.4%	-15.5%	-1.8%	-3.1%	-1.0%	-1.9%	-0.3%	-3.0%	-5.2%	-14.8%
NP_90-2	+	-1.3%	-3.0%	0.2%	0.0%	0.5%	-1.4%	/	/	-1.9%	-3.3%	0.4%	0.2%	1.1%	-1.3%	/	/
	-	0.2%	0.4%	0.4%	-0.1%	-5.0%	-9.8%	/	/	0.3%	0.5%	0.3%	0.1%	-6.2%	-11.3%	/	/
RNP_0-1	+	-1.8%	-2.7%	0.8%	0.6%	2.8%	0.9%	-8.8%	-15.5%	-1.9%	-2.8%	0.7%	0.4%	3.4%	1.0%	-8.2%	-15.4%
	-	-0.1%	-0.3%	0.2%	0.2%	-2.0%	-5.8%	-8.2%	-22.5%	-0.1%	-0.4%	0.6%	0.5%	-2.1%	-5.4%	-7.9%	-21.3%
RNP_0-2	+	-0.9%	-0.3%	1.1%	0.8%	3.5%	2.7%	-10.7%	-17.5%	-0.6%	-0.7%	0.9%	0.9%	3.6%	3.2%	-9.5%	-16.8%
	-	-1.0%	-1.3%	-0.2%	-0.7%	-1.5%	-9.3%	-4.8%	-9.5%	-1.2%	-1.7%	-0.4%	-0.7%	-1.6%	-10.3%	-5.2%	-9.4%
RNP_90-1	+	0.5%	-0.2%	0.9%	0.6%	3.5%	3.1%	-15.2%	-43.1%	0.4%	-0.3%	0.7%	0.5%	3.4%	3.1%	-15.8%	-45.2%
	-	-2.6%	-4.8%	-0.7%	-1.4%	-1.0%	-3.7%	-16.8%	-104.1%	-2.4%	-3.8%	-0.9%	-1.4%	-1.0%	-3.6%	-16.6%	-103.8%
RNP_90-2	+	3.0%	2.4%	4.9%	5.0%	2.1%	2.7%	-12.2%	-21.1%	3.2%	2.4%	4.7%	5.0%	2.0%	2.9%	-11.5%	-20.2%
	-	-2.2%	-2.8%	-0.9%	-1.8%	2.7%	-1.0%	-5.4%	-65.0%	-2.1%	-2.9%	-0.8%	-1.7%	2.4%	-1.1%	-5.1%	-65.3%
SB_0-1	+	-1.3%	-2.0%	0.7%	-0.1%	1.5%	1.4%	-0.5%	-7.5%	-1.0%	-1.6%	0.7%	0.0%	1.4%	1.2%	-0.3%	-7.4%
	-	-2.0%	-3.3%	-1.8%	-2.8%	-0.1%	-0.7%	-9.1%	-17.1%	-1.9%	-3.1%	-1.9%	-2.9%	-0.4%	-0.8%	-9.2%	-17.3%
SB_0-2	+	-0.9%	-2.3%	-0.5%	-1.2%	1.4%	1.1%	-0.6%	-5.7%	-3.4%	-5.1%	-0.4%	-1.2%	1.2%	0.9%	-0.6%	-5.3%
	-	-2.2%	-3.1%	-1.8%	-3.1%	-0.6%	-1.2%	-6.2%	-12.8%	-2.3%	-3.3%	-1.9%	-3.1%	-0.7%	-1.4%	-6.7%	-13.1%
SB_90-1	+	-1.2%	-1.7%	-1.6%	-2.8%	1.9%	1.6%	-5.2%	-12.1%	-1.1%	-1.7%	-1.8%	-2.8%	1.9%	1.7%	-4.8%	-11.7%
	-	-0.9%	-3.3%	-1.0%	-1.3%	0.3%	0.0%	-10.7%	-16.4%	-1.0%	-3.0%	-1.0%	-1.4%	0.3%	-0.1%	-10.8%	-16.2%
SB_90-2	+	-1.3%	-1.8%	-2.0%	-3.1%	-2.0%	-2.4%	0.0%	-5.6%	-1.4%	-2.0%	-2.2%	-3.3%	-2.1%	-2.4%	-0.6%	-5.3%
	-	-1.7%	-2.9%	-1.8%	-2.9%	-0.6%	-1.2%	-6.2%	-12.8%	-1.5%	-2.5%	-1.8%	-2.8%	-0.4%	-1.1%	-6.7%	-13.0%

4.3. Equivalent viscous damping ratio

The performances in terms of energy dissipation were evaluated through the calculation of the viscous damping ratio *v* according to EN 12512 [31] (Table 5). The load cycles up to $d_{y,est}$, although included in the analysis, were less interesting due to the limited dissipated energy content in those cycles. With reference to $d > d_{y,est}$, the NP and RNP fastenings provided damping ratios up to 30% and 40% for the 20- and 30-mm displacement amplitude, respectively. The elastic response of the SB solution affected the damping ratio evaluation with *v* values limited to 20 and 30% for the same displacement level.

Setting the viscous damping ratio of the rigid joint configuration as common denominator for the whole damping values, it can be observed that the three analysed fastenings provided less dissipating capacity at the lowest displacements ($\eta_v < 1$) and performed equally or better only at the largest displacements (Fig. 13). Even if results for the first tests only are shown in Fig. 13, this observation is valid for both test runs.

Table 5. Equivalent Viscous Damping ratio calculated at each significant displacement level.

		3.75 mm			5 mm			10 mm			20 mm			30 mm		
		1st Cycle	2nd Cycle	3rd Cycle	1st Cycle	2nd Cycle	3rd Cycle	1st Cycle	2nd Cycle	3rd Cycle	1st Cycle	2nd Cycle	3rd Cycle	1st Cycle	2nd Cycle	3rd Cycle
Rigid	+	5%	9%	9%	10%	13%	13%	21%	24%	24%	29%	35%	36%	37%	32%	30%
	-	8%	8%	9%	11%	13%	13%	24%	24%	21%	35%	35%	42%	36%	31%	31%
NP_0-1	+	21%	20%	21%	17%	18%	17%	14%	14%	14%	24%	28%	28%	36%	37%	/
	-	21%	21%	21%	18%	17%	17%	15%	14%	14%	29%	28%	28%	41%	39%	/
NP_0-2	+	28%	28%	27%	22%	21%	21%	13%	12%	13%	22%	28%	27%	35%	/	/
	-	23%	21%	22%	18%	17%	17%	14%	12%	12%	28%	27%	27%	45%	/	/
NP_90-1	+	15%	14%	14%	13%	13%	12%	17%	17%	15%	26%	28%	27%	34%	33%	31%
	-	19%	18%	18%	15%	14%	14%	18%	15%	15%	28%	27%	27%	33%	30%	32%
NP_90-2	+	14%	12%	12%	13%	12%	11%	17%	17%	17%	30%	32%	32%	/	/	/
	-	16%	16%	15%	13%	13%	12%	17%	16%	15%	30%	30%	29%	/	/	/
RNP_0-1	+	13%	12%	11%	12%	12%	12%	19%	19%	18%	30%	33%	32%	40%	38%	35%
	-	20%	19%	19%	17%	16%	16%	21%	19%	19%	33%	33%	32%	40%	37%	35%
RNP_0-2	+	17%	16%	16%	13%	13%	12%	14%	13%	14%	25%	29%	29%	38%	36%	33%
	-	16%	15%	15%	13%	12%	12%	17%	15%	15%	31%	31%	31%	39%	35%	33%
RNP_90-1	+	13%	12%	12%	10%	9%	9%	13%	12%	13%	24%	28%	27%	34%	36%	39%
	-	15%	14%	14%	12%	10%	10%	16%	14%	13%	30%	29%	28%	39%	36%	39%
RNP_90-2	+	21%	21%	20%	17%	16%	16%	12%	11%	13%	23%	29%	27%	35%	35%	32%
	-	15%	14%	13%	12%	11%	11%	17%	14%	13%	31%	29%	29%	38%	34%	44%
SB_0-1	+	12%	12%	12%	11%	10%	10%	9%	9%	7%	16%	18%	17%	23%	25%	23%
	-	13%	12%	12%	11%	11%	10%	10%	8%	8%	20%	17%	17%	27%	25%	23%
SB_0-2	+	11%	12%	11%	11%	11%	11%	8%	7%	7%	12%	14%	13%	19%	23%	20%
	-	13%	12%	11%	11%	10%	10%	9%	7%	6%	17%	14%	13%	25%	22%	21%
SB_90-1	+	8%	7%	7%	7%	6%	6%	9%	8%	7%	17%	19%	18%	24%	28%	26%
	-	23%	20%	20%	15%	14%	14%	10%	9%	8%	21%	19%	19%	30%	29%	28%
SB_90-2	+	11%	10%	10%	9%	8%	8%	11%	9%	9%	16%	14%	13%	19%	22%	20%
	-	19%	18%	17%	14%	13%	12%	12%	10%	9%	17%	14%	13%	25%	22%	21%

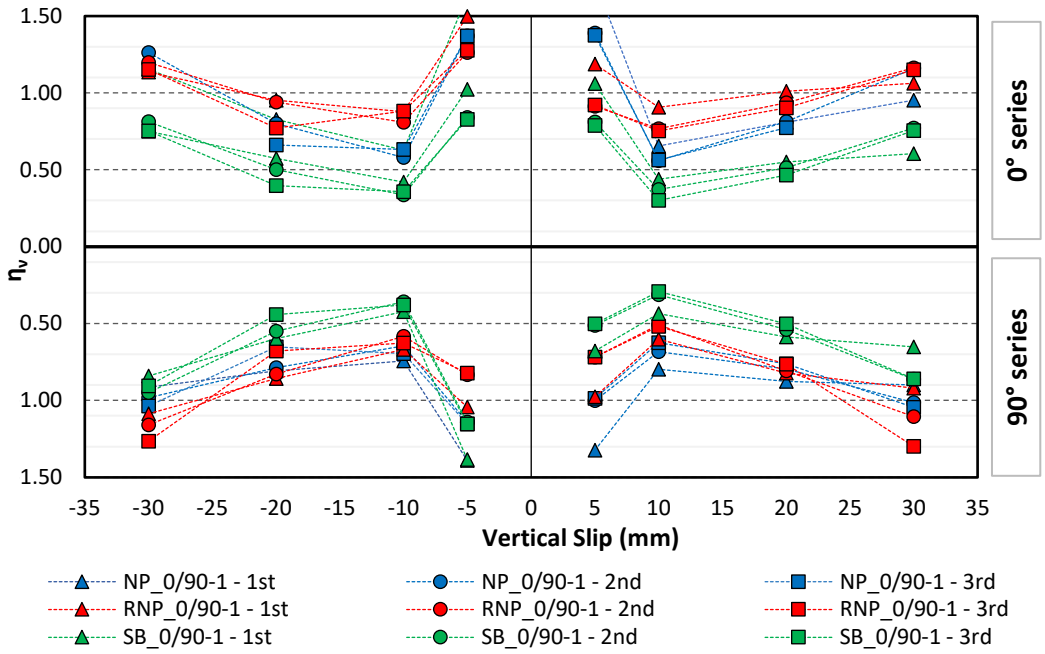

Fig. 13. Ratio of the viscous damping between semirigid and rigid anchoring solution at significant displacement levels for the first test run.

5. Conclusions

The study presented the results of an experimental campaign, in which twelve cyclic tests were performed on panel-to-panel shear connections composed by high-ductility X-bracket steel dampers connected to CLT panels with three different fastening types: nailed plate (NP), nailed plate reinforced with carbon fabric (RNP) and screwed plastic bushings (SB). The direction of the outer layer of boards (0° or 90°) with respect to the main loading direction was also accounted for as an additional variable. After the first test run, stopped in correspondence of the failure of one of the X-bracket, all the metallic parts of the connections were substituted, confirming an easy replaceability of the fuse, and the test was repeated.

Results were reported in terms of global and local response of the connection to investigate similarities and differences between the fastening types. In all the tests, the yielding of the dampers was activated, achieving inelastic deformations of the steel elements and registering large slips at the panel-to-panel interface. In general, the global response was characterized by large inelastic deformations and dissipated energy. The different fastenings affected the capacity of the whole connection assembly as they reached different imposed displacement amplitude before the failure of the dampers. In more detail, the SB fastening was characterized by a larger displacement capacity. Significant differences were not observed in the second test runs. At the end of the tests, local residual damages were only noticed for the NP solution, with the yielding of nails and wood embedment.

In terms of local response of the different fastening types, differences were observed for the SB fastening between the two considered directions of the outer layer of boards with respect to the loading direction, due to the differences, in terms of stiffness, between the bushings and the wood parallel or perpendicular to the grain.

The mechanical properties of the whole connection, such as elastic stiffness, yielding point and ductility were determined considering a trilinear approximation of the global load-displacement behaviour. In general, the RNP solution was characterized by the highest elastic stiffness, while the SB fastening was characterized by the lowest value. Comparison with analytical formulations for the evaluation of the stiffness of the connections, according to a model of elastic springs working in series, provided a good agreement. In terms of ductility, the use of different fastenings led to different ductility classes. In more detail, the RNP fastening was the one having the highest ductility, while unsatisfactory results were obtained for the NP connection, due to the shift of the yielding displacement, and for second test runs. Significant force and secant stiffness degradation were only observed in some cases at high displacement amplitude, especially for the RNP solution. The equivalent viscous damping was evaluated as well.

In comparison with the results obtained with the same damper rigidly fastened to a steel frame, the experimental outcomes evidenced how the performance of a damper for earthquake resistant CLT structures may be affected by the deformability and cyclic response of fastenings, even if fulfilling the capacity design criteria. Therefore, capacity design rules applied to the fastening elements of a dissipating system should provide also requirements in terms of minimal stiffness ratio. Indeed, low elastic stiffness anchoring solutions enable higher displacements, altering the static ductility values and the viscous damping ratio of the connection.

Acknowledgements

The financial support of TIRISICO Project (POR FESR 2014-2020 – Regione Emilia Romagna) and of (Italian) Department of Civil Protection (ReLUIS 2022-2024 Grant – Innovative Materials) are gratefully acknowledged.

References

1. Sarti F, Palermo A, Pampanin S (2015) Development and Testing of an Alternative Dissipative Posttensioned Rocking Timber Wall with Boundary Columns. Journal of Structural Engineering 142:E4015011. https://doi.org/10.1061/(ASCE)ST.1943-541X.0001390
2. Chen Z, Popovski M, Iqbal A (2020) Structural Performance of Post-Tensioned CLT Shear Walls with Energy Dissipators. Journal of Structural Engineering 146:04020035. https://doi.org/10.1061/(ASCE)ST.1943-541X.0002569
3. Hashemi A, Quenneville P (2020) Large-scale testing of low damage rocking Cross Laminated Timber (CLT) wall panels with friction dampers. Engineering Structures 206:110166. https://doi.org/10.1016/J.ENGSTRUCT.2020.110166
4. Pozza L, Benedetti L, Tomei V, et al (2021) Cyclic response of CLT Post-Tensioned Walls: Experimental and numerical investigation. Construction and Building Materials 308:125019. https://doi.org/10.1016/j.conbuildmat.2021.125019
5. Hashemi A, Yousef-Beik SMM, Mohammadi Darani F, et al (2019) Seismic performance of a damage avoidance self-centring brace with collapse prevention mechanism. Journal of Constructional Steel Research 155:273–285. https://doi.org/10.1016/j.jcsr.2018.12.019
6. Hashemi A, Quenneville P (2020) Large-scale testing of low damage rocking Cross Laminated Timber (CLT) wall panels with friction dampers. Engineering Structures 206:110166. https://doi.org/10.1016/J.ENGSTRUCT.2020.110166
7. Pampanin S, Arup JC, Bianchi S, et al (2020) Seismic Safety and Reducing Seismic Losses: Overview and Preliminary Results of SERA Project-3D Shaking Table Tests on An Integrated Low-Damage …. In: 17th World Conference on Earthquake Engineering. Sendai, Japan
8. Trutalli D, Marchi L, Scotta R, Pozza L (2019) Capacity design of traditional and innovative ductile connections for earthquake-resistant CLT structures. Bulletin of Earthquake Engineering 17:2115–2136. https://doi.org/10.1007/s10518-018-00536-6
9. Follesa M, Fragiacomo M, Casagrande D, et al (2018) The new provisions for the seismic design of timber buildings in Europe. Engineering Structures 168:736–747. https://doi.org/10.1016/j.engstruct.2018.04.090
10. Santos CL, de Jesus AMP, Morais JJL, Fontoura BFC (2013) An experimental comparison of strengthening solutions for dowel-type wood connections. Construction and Building Materials 46:114–127. https://doi.org/10.1016/j.conbuildmat.2013.03.021
11. Bellini A, Benedetti L, Pozza L, Mazzotti C (2020) Experimental characterization of monotonic and cyclic behavior of steel-to-CLT nailed joints strengthened with composite plies. Construction and Building Materials 256:119460. https://doi.org/10.1016/j.conbuildmat.2020.119460
12. Ringhofer A, Brandner R, Blaß HJ (2018) Cross laminated timber (CLT): Design approaches for dowel-type fasteners and connections. Engineering Structures 171:849–861. https://doi.org/10.1016/j.engstruct.2018.05.032
13. Heiduschke A, Haller P (2008) Performance of composite-reinforced timber joints using single dowel-type fasteners. In: 10th World Conference on Timber Engineering (WCTE). Miyazaki, Japan

14. Larsson G, Serrano E, Gustafsson PJ, Danielsson H (2020) Dowel design of the shear plate dowel joint. Engineering Structures 209:110296. https://doi.org/10.1016/j.engstruct.2020.110296
15. Rodd PD, Leijten AJM (2003) High-performance dowel-type joints for timber structures. Progress in Structural Engineering and Materials 5:77–89. https://doi.org/10.1002/pse.144
16. Santos CL, de Jesus AMP, Morais JJL, Fontoura BFC (2013) An experimental comparison of strengthening solutions for dowel-type wood connections. Construction and Building Materials 46:114–127. https://doi.org/10.1016/j.conbuildmat.2013.03.021
17. Yang JQ, Smith ST, Wu YF, Feng P (2020) Strengthening single-bolt timber joints with externally bonded CFRP composites. Structures 28:2671–2685. https://doi.org/10.1016/j.istruc.2020.10.024
18. Heiduschke A, Haller P (2008) Performance of composite-reinforced timber joints using single dowel-type fasteners. In: 10th World Conference on Timber Engineering (WCTE)
19. CEN (2005) EN 1995-1-2 Eurocode 5: Design of timber structures - Part 1-2: General - Structural fire design. Brussels, Belgium
20. CEN (2012) EN 912 Timber fasteners Specifications for connectors for timbers. Brussels, Belgium
21. Pavković K, Rajčić V, Haiman M (2014) Large diameter fastener in locally reinforced and non-reinforced timber loaded perpendicular to grain. Engineering Structures 74:256–265. https://doi.org/10.1016/j.engstruct.2014.05.046
22. Crocetti R, Axelson M, Sartori T (2010) Strengthening of large diameter single dowel joints. SP Report 2010:14, SP Technical Research Institute of Sweden.
23. Asgari H, Tannert T, Loss C (2022) Block tear-out resistance of CLT panels with single large-diameter connectors. European Journal of Wood and Wood Products 1–12. https://doi.org/10.1007/S00107-022-01809-3/FIGURES/9
24. CEN (2004) EN 10025-2 Hot rolled products of structural steels - Technical delivery conditions for non-allow structural steels. Brussels, Belgium
25. Marchi L, Trutalli D, Scotta R, Pozza L (2020) Macro-element modelling of a dissipative connection for CLT structures. Structures 26:582–600. https://doi.org/10.1016/j.istruc.2020.04.044
26. CEN (2016) EN 338 Structural timber — Strength classes. Brussels, Belgium
27. OIB (2018) ETA-12/0281 Cross Laminated Timber (CLT) – Solid wood slab elements to be used as structural elements in buildings. Wien
28. CEN (2016) EN 384 Structural timber - Determination of characteristic values of mechanical properties and density. Brussels, Belgium
29. ETA-Danmark (2019) ETA-04/0013. Nails and screws for use in nailing plates in timber structures. Copenhagen
30. CEN (2009) EN 409 Timber structures – Test methods – Determination of the yield moment of dowel type fasteners. Brussels, Belgium
31. CEN (2011) EN 12512 Timber structures-Test methods: Cyclic testing of joints made with mechanical fasteners. Brussels, Belgium
32. Scotta R, Marchi L, Trutalli D, Pozza L (2016) A Dissipative Connector for CLT Buildings: Concept, Design and Testing. Materials 9:139. https://doi.org/10.3390/ma9030139
33. Muñoz W, Mohammad M, Salenikovich M, Quenneville P (2008) Need for a harmonized approach for calculations of ductility of timber assemblies. In: CIB W18 Meeting
34. Pozza L, Saetta A, Savoia M, Talledo D (2017) Coupled axial-shear numerical model for CLT connections. Construction and Building Materials 150:568–582. https://doi.org/10.1016/j.conbuildmat.2017.05.141